Analysis of strong ionospheric scintillation events measured by means of GPS signals at low latitudes during disturbed conditions

B. Forte[1,2]

Received 4 June 2011; revised 3 May 2012; accepted 23 May 2012; published 25 August 2012.

[1] Drifting structures characterized by inhomogeneities in the spatial electron density distribution at ionospheric heights cause the scintillation of radio waves propagating through. The fractional electron density fluctuations and the corresponding scintillation levels may reach extreme values at low latitudes during high solar activity. Different levels of scintillation were observed on experimental data collected in the Asian sector at low latitudes by means of a GPS dual frequency receiver under moderate solar activity (2005). The GPS receiver used in these campaigns was particularly modified in firmware in order to record power estimates on the C/A code as well as on the carriers L1 and L2. Strong scintillation activity was recorded in the post-sunset period (saturating S_4 and *SI* as high as 20 dB). Spectral modifications and broadening was observed during high levels of scintillation possibly indicating refractive scattering taking place instead of diffractive scattering. A possible interpretation of those events was attempted on the basis of the refractive scattering theory developed by Uscinski (1968) and Booker and MajidiAhi (1981).

Citation: Forte, B. (2012), Analysis of strong ionospheric scintillation events measured by means of GPS signals at low latitudes during disturbed conditions, *Radio Sci.*, *47*, RS4009, doi:10.1029/2011RS004789.

1. Introduction

[2] Electromagnetic waves propagating through an irregular medium may be scattered by refractive index fluctuations. In the presence of small angle scattering, intensity and phase fluctuations may be observed on the received waves after propagating through such spatial inhomogeneities in the refractive index.

[3] Usually, two types of scattering are considered for the scintillation of radio waves: weak scattering (occurring for low scintillation levels) and strong scattering (occurring for high and saturating scintillation levels, $S_4 \sim 1$) [*Yeh and Liu*, 1982; *Rino*, 1979a, 1979b]. The problem is often modeled by means of a thin phase changing screen which allows for both weak and strong scattering to be easily described. Diffractive scattering is due to refractive index inhomogeneities with scales smaller than the Fresnel scale corresponding to the propagation problem. Diffractive scattering usually dominates when the spatial refractive index fluctuations are relatively low. On the contrary, when they are large, a refractive type of scattering appears to be the dominant mechanism. Refractive scattering is produced by spatial refractive index inhomogeneities with scales larger than the Fresnel scale. When refractive scattering dominates, besides the usual Fresnel scale associated with the propagation problem, other scales (such as the peak scale, the focal scale, and the lens scale) come into play [*Uscinski*, 1968; *Booker and MajidiAhi*, 1981].

[4] Experimental evidence of scintillation events dominated by a refractive type of scattering was found at low latitudes [*Vats et al.*, 1981; *Crain et al.*, 1979] and at high latitudes [*Forte*, 2008]. In those cases the evidence was based on beacon signals at VHF and UHF wavelengths broadcast from geostationary satellites [*Vats et al.*, 1981; *Crain et al.*, 1979] as well as from polar orbiting low Earth orbiting satellites [*Forte*, 2008]. Those signals traversed ionospheric plasma density structures with particularly large fluctuations in the spatial electron density distribution to cause a refractive type of scattering. The specific signature of refractive scattering was identified in the power spectral density estimates of the received intensity, which showed a broadening toward higher and lower fluctuation frequencies [*Uscinski*, 1968; *Booker and MajidiAhi*, 1981].

[5] Here, GPS based intensity and phase measurements during high scintillation were analyzed in order to understand whether any signature of refractive scattering might be identified. Estimates of the intensity power spectral density were calculated directly from experimental data and compared with

[1]Institute of Engineering Surveying and Space Geodesy, University of Nottingham, Nottingham, UK.
[2]Centre for Atmospheric Research, University of Nova Gorica, Nova Gorica, Slovenia.

Corresponding author: B. Forte, Centre for Atmospheric Research, University of Nova Gorica, Vipavska 13, SI-5000, Nova Gorica, Slovenia. (biagio.forte@ung.si)

0048-6604/12/2011RS004789

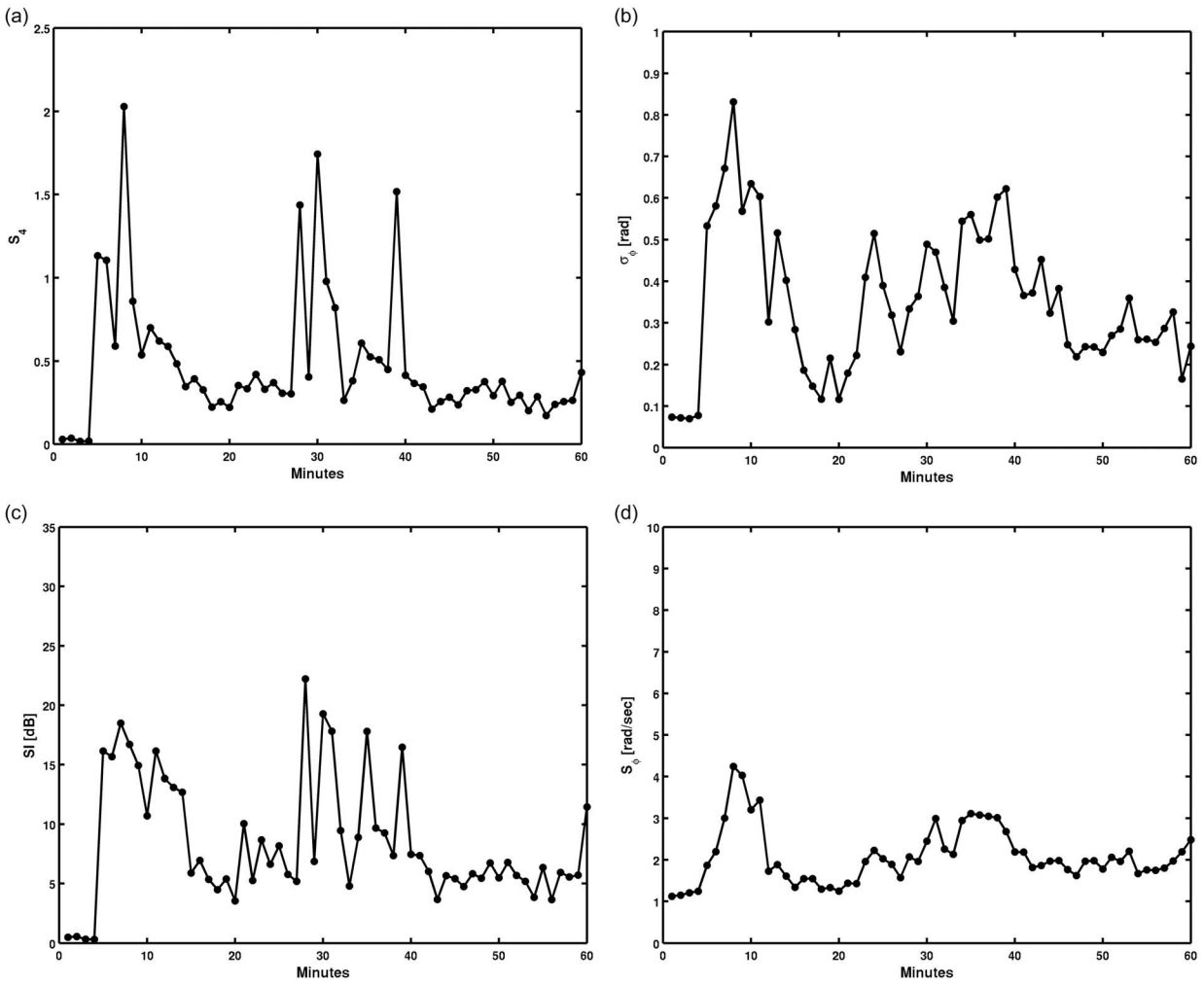

Figure 1. The scintillation indices S_4, σ_ϕ, SI, and S_ϕ for PRN30 at L1 between 18:00LT and 19:00LT as observed from Bandung on 6 April 2005.

numerical spectra resulting from the theory outlined in *Booker and MajidiAhi* [1981].

[6] Previous studies analyzed spectral features on scintillating GPS signals, as well. In particular, some analyses considered a statistical description of those spectral features essentially based on a weak scattering assumption [*Van de Kamp and Cannon*, 2009], while others indeed acknowledged spectral broadening occurring in the presence of high scintillation levels on GPS signals, though the authors were not interested in the ultimate scattering mechanism producing those signatures but only in fitting their numerical model to the experimental data [*Humphreys et al.*, 2009].

2. The Data Set and the Events Considered

[7] The data set referred to measurements collected during a campaign run on 6 April 2005 at Bandung (geographic latitude 6.9 *S*, geographic longitude 107.6 *E*, magnetic dip $\approx -16.5°$) by using a dual frequency GPS receiver (Topcon GB-1000), suitably modified to produce GPS data at a sampling rate of 25 Hz together with estimates of the received signals intensities (the receiver did not output C/N_0 but estimates of the signal intensity) (N. Jakowski, private communication, 2009). The magnetic conditions were disturbed with the planetary K_p index reaching a peak value of 7.0 in that day. Classical scintillation indices such as the normalized second moment of the received intensity S_4 [*Briggs and Parkin*, 1963] and the second moment of the received phase σ_ϕ [*Fremouw et al.*, 1978] were calculated as temporal averages over 1-minute intervals by assuming ergodic processes. In addition, peak-to-peak fluctuations in dB were quantified by means of the *SI* index [*Whitney and Chester*, 1968], while phase dynamics was evaluated by means of the second moment of the first time derivative of the received phase S_ϕ [*Forte*, 2005] again by assuming ergodicity. The experimental setup as well as the calculation of the scintillation parameters was similar to that of another experiment done at high latitudes run in 2003 [*Forte*, 2005].

[8] The 25 Hz carrier phase samples were spectrally processed in order to separate high from low fluctuation frequency components. This was accomplished by means of a finite impulse response Butterworth filter with a low-frequency detrending cut-off of 0.1 Hz, in total analogy with the method implemented within typical GPS scintillation monitors [*Van Dierendonck et al.*, 1993]. The detrending was operated

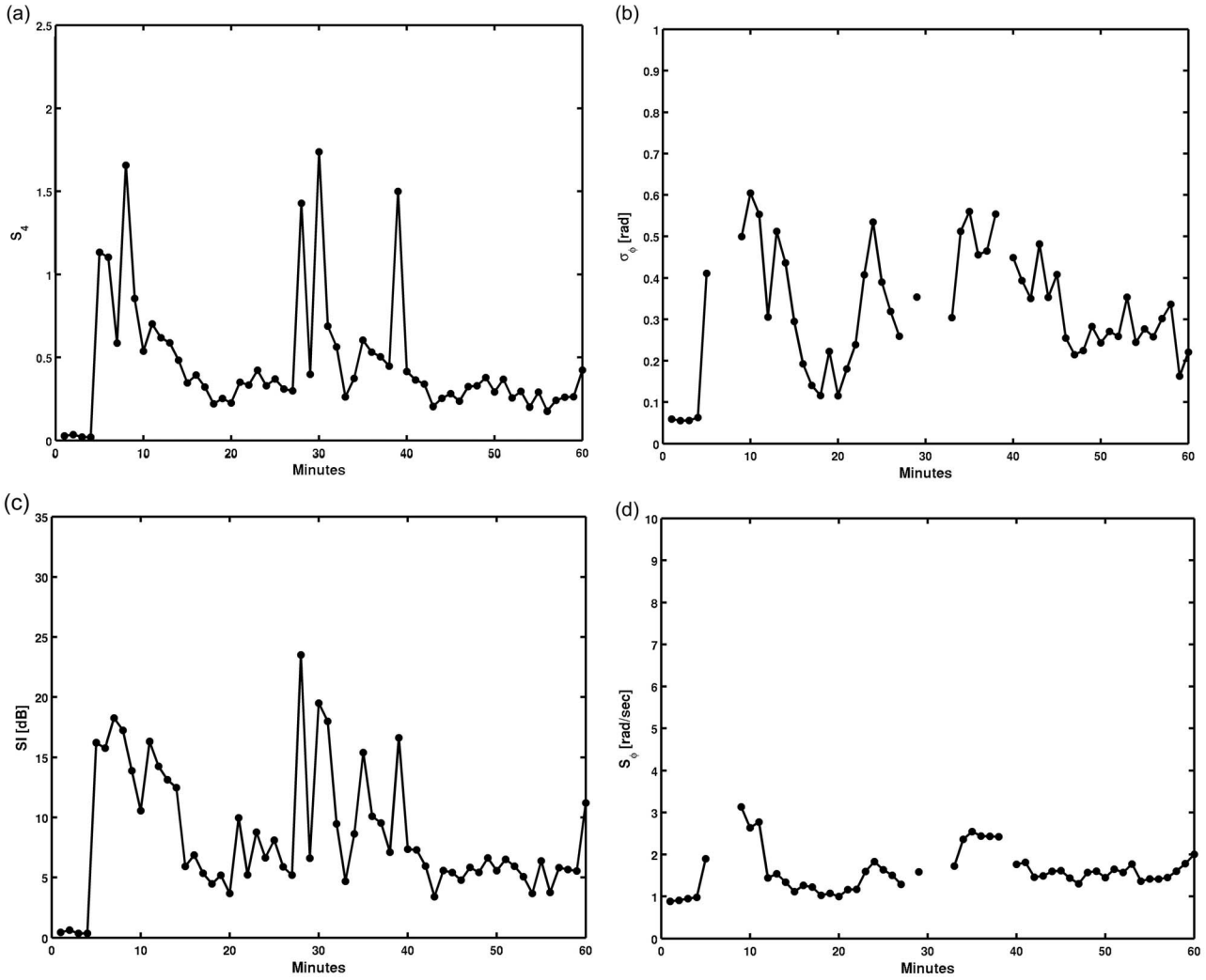

Figure 2. The scintillation indices S_4, σ_ϕ, *SI*, and S_ϕ for PRN30 at L2 between 18:00LT and 19:00LT as observed from Bandung on 6 April 2005.

on each individual 1-minute interval of data leading to scintillation indices averaged over that period. On the other hand, the intensity scintillation index S_4 was calculated as the standard deviation of the normalized intensity, without any detrending process, again in total analogy with typical GPS scintillation monitors [*Van Dierendonck et al.*, 1993]. The *SI* index was calculated on the raw 25 Hz intensity estimates for each particular PRN signal, without any prior detrending. Finally, the S_ϕ index was calculated as the standard deviation of the first time derivative of the carrier phase. It was shown S_ϕ to be independent on low-frequency fluctuations and consequently on detrending, which may indicate it as a more robust measurement of phase scintillation [*Forte*, 2005].

[9] A representative event of data measured on 6 April 2005 is shown in the summary plots in Figures 1 and 2, which pertains to the GPS signals received from satellite PRN30 between 18:00LT and 19:00LT. The plots in Figure 1 refer to the indices calculated from the intensity and phase estimates at L1, while the plots in Figure 2 refer to the indices calculated for L2. The results for L1 and L2 appeared to be very similar though not the same. The signal fluctuations seemed to be very similar on both L1 and L2 (with individual fades deeper on L2 though), showing a high degree of correlation in terms of scintillation indices. The reason for this could be possibly attributed in part to semi-codeless tracking of L2 and to the subsequent reconstruction utilized to estimate the signal level and in part to the possible presence of refractive scattering. From the point of view of the receiver response, the scintillation appeared well correlated on both L1 and L2.

[10] For the event in Figures 1 and 2, an initial period of very low scintillation activity (indices very small in view of low fluctuations with high C/N_0 being tracked from PRN30) was followed by two significant enhancements in the scintillation activity which were recorded around minutes 5 and 30 of the one hour period considered. At these times S_4 exceeded unity on both L1 and L2 approaching values in excess of 1.8 with several fades present in those particular minutes. During the remaining part of that hour, the S_4 scintillation index showed values as low as 0.3. The scintillation activity depicted by the S_4 index closely resembled the trend of the *SI*-index, though peak-to-peak fluctuations

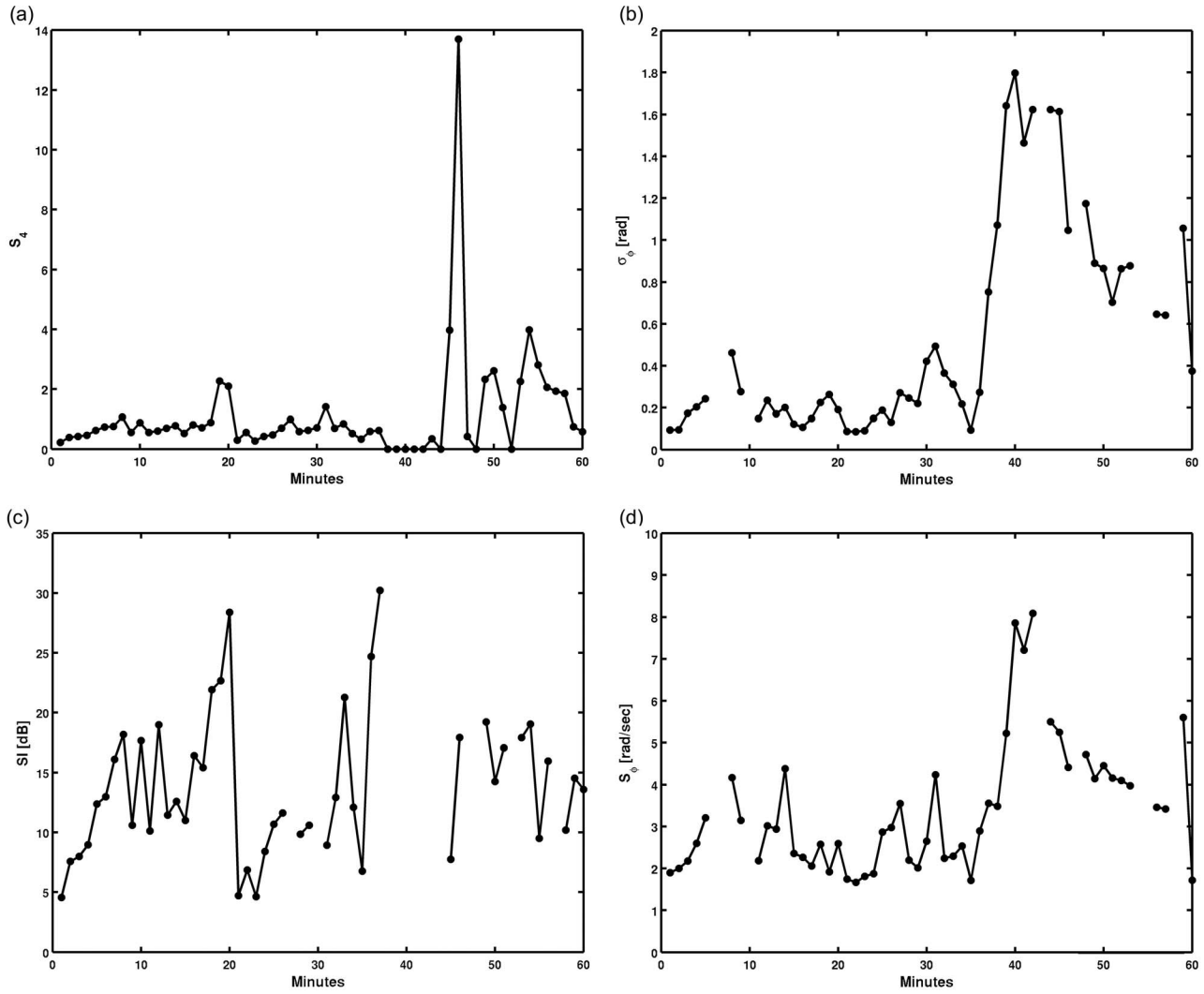

Figure 3. The scintillation indices S_4, σ_ϕ, *SI*, and S_ϕ for PRN01 at L1 between 20:00LT and 21:00LT as observed from Bandung on 6 April 2005.

around minute 5 ($S_4 \leq 2$) were of the order of 20 dB and in excess of 20 dB around minute 30 ($S_4 \leq 1.8$). The classical phase scintillation index σ_ϕ showed a similar trend, though with some data gaps on L2 due to more frequent losses of lock in that particular interval. The initial enhancement corresponded to a σ_ϕ in excess of 0.8 rad on L1 and smaller than 0.7 rad on L2. In the remaining part of that hour σ_ϕ showed values between 0.1 rad and 0.5 rad, with larger values on L1. A clearer trend was evident on the S_ϕ-index which appeared to closely follow the trends of both S_4 and *SI*, with peak values between 3 rad/s and 4 rad/s in correspondence of maximum scintillation activity.

[11] Additional examples of the events recorded between 18:00LT and 19:00LT, when the scintillation activity was particularly intense, are shown in Figures 3–6, for PRN01 (Figure 3), PRN03 (Figure 4), PRN14 (Figure 5), and PRN22 (Figure 6). All the plots in Figures 3–6 refer to scintillation indices on L1 only. Some PRNs showed moderate to high scintillation activity, while others showed low to moderate scintillation activity, as a result of the different raypath geometries for the satellites considered and the inhomogeneities in the ionospheric electron density. The plots scales in Figures 3–6 are not the same in order to offer a detailed view on the upper values observed.

[12] Data gaps may be observed in Figures 1–6. Some of the gaps were due to temporary losses of lock (Figures 2, 3, and 5), while others were due to the lack of convergence of the detrending methods owing to gaps present already in the original data (see Figure 3 in correspondence of σ_ϕ and Figure 8 for the detrended L1 carrier phase). The scintillation indices were calculated over all available data points in a given minute. On the other hand, in the case of non-convergence of data detrending methods (owing to gaps in the original data possibly because of temporary losses of lock) a particular minute was left entirely empty, resulting in a data gap in the phase scintillation index.

[13] A detail of the fades on the signals measured from PRN30 and PRN01 is offered in Figures 7 and 8. The 25 Hz non-detrended intensity and detrended L1 carrier phase are shown for the two PRNs. The raw signal recorded from

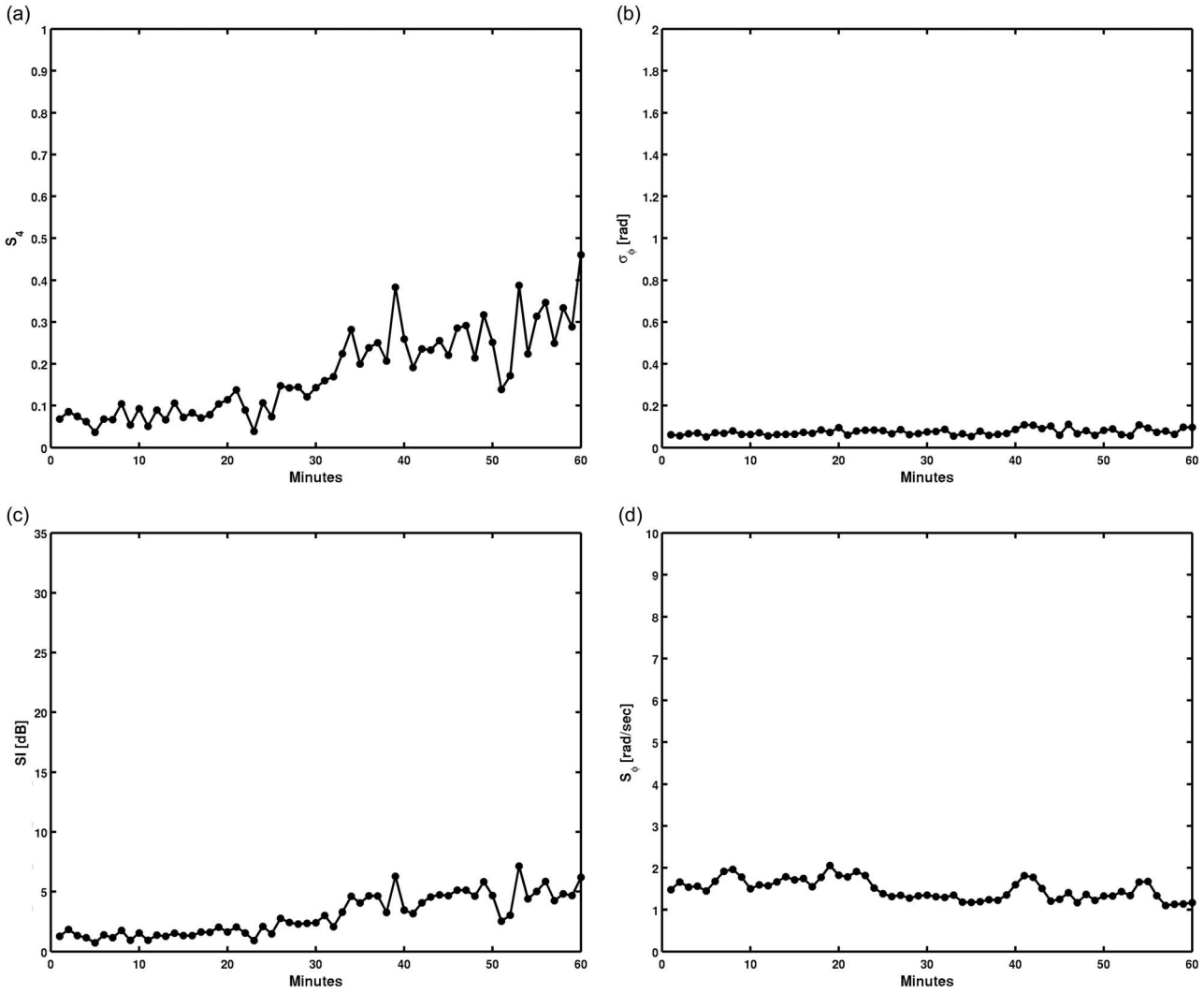

Figure 4. The scintillation indices S_4, σ_ϕ, SI, and S_ϕ for PRN03 at L1 between 20:00LT and 21:00LT as observed from Bandung on 6 April 2005.

PRN01 showed larger gaps in the received intensity than on the received L1 carrier phase (the high-frequency component of which is only shown), which may be associated to internal logics within the particular type of receiver used to estimate the signal level. In this case, the presence of strong scintillation on PRN01 made the receiver tracking scheme capable of estimating the L1 carrier phase for longer periods than those over which the signal level could be appreciated. The isolated peak in S_4 for PRN01 (Figure 3) was probably not correct due to large gaps in the estimate of the signal intensity, implying fewer data points over which S_4 was calculated. On the other hand, the remaining values of S_4 proved consistent with the original 25 Hz signal intensity measurements. The larger fluctuations on the high-frequency component of the L1 carrier phase after minute 35 (Figure 8) may be associated with scintillation enhancements as well as with high non-linearity in the tracking scheme implemented in the receiver. Gaps around minutes 6 and 9 were introduced by the fact that the detrending method did not converge because of gaps in the original time series (probably owing to short losses of lock). As a consequence, the entire minutes were left empty in the time series of the detrended carrier phase, which further introduced gaps in the phase scintillation indices.

3. Discussion

[14] Figure 9 shows the power spectral densities (PSD) of the received intensity on the L1 signals for the event shown in Figures 1–6. Figure 9a shows the PSD for PRN30 during the period 18:00 to 19:00 LT, Figure 9b refers to PRN01 during the same period; Figure 9c is for PRN03, Figure 9d is for PRN14, and finally Figure 9e is for PRN22. In Figure 9, blue correspond to 10^{-8} and red to 10^{3} in units of S_4^2/Hz. Spectral modifications were evident on the signals from all satellites in view and the extent of modification was related to the different levels of scintillation (compare Figure 9 with Figures 1–6 for corresponding PRNs). Some of those modifications appeared more marked than others which was possibly due to different scattering mechanisms taking place. For the signals from those satellites which encountered a high to saturating scintillation level (i.e., PRNs 30, 01, 14), the spectral modifications consisted of an increase of the

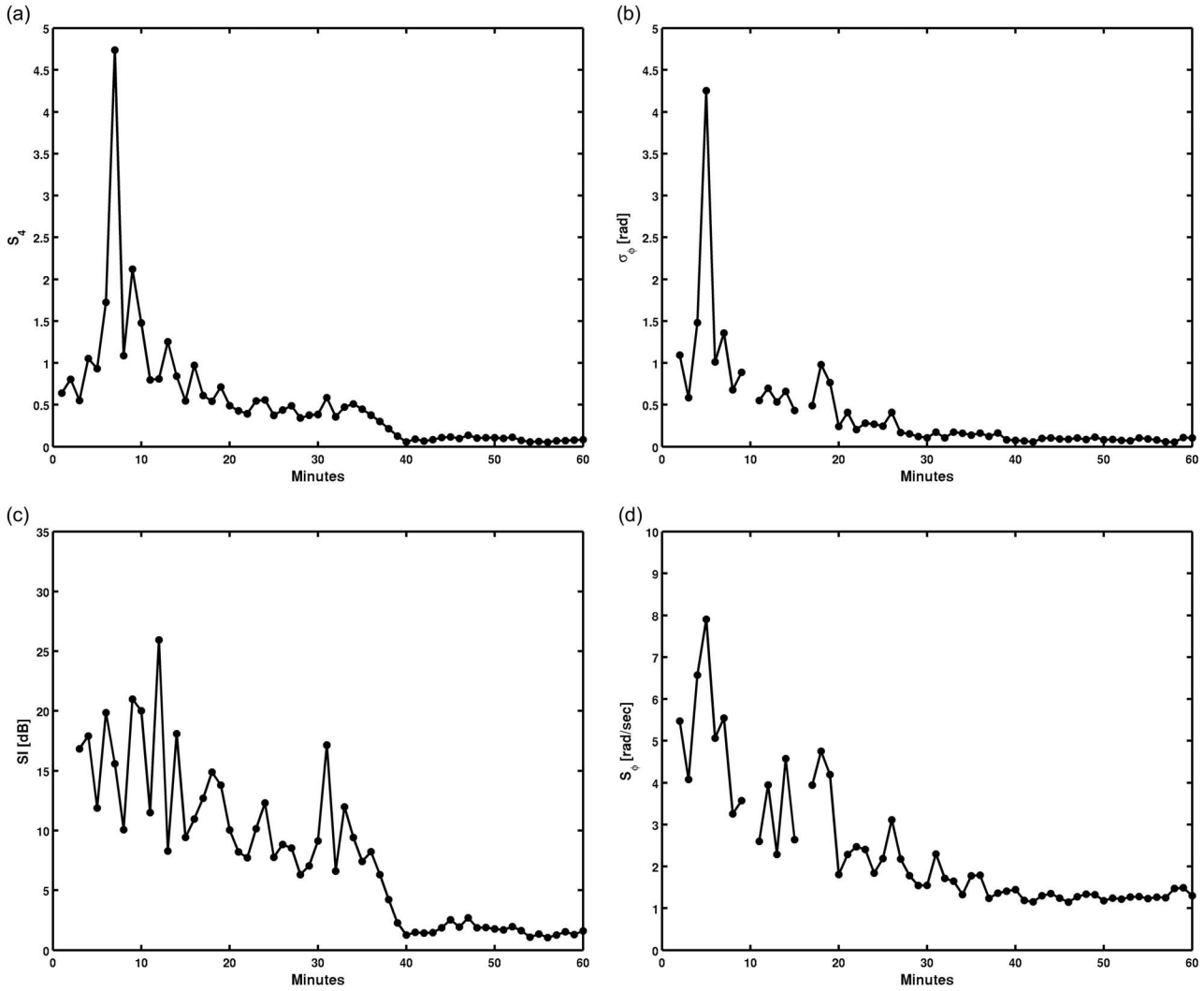

Figure 5. The scintillation indices S_4, σ_ϕ, SI, and S_ϕ for PRN14 at L1 between 20:00LT and 21:00LT as observed from Bandung on 6 April 2005.

PSD level together with its expansion toward higher fluctuation frequencies. Actually, such an expansion would be expected even toward lower fluctuation frequencies. However, this could not be observed as satellite motion posed a lower limit to the resolvable spectral window. White strips appearing on some of the PSD plots are due to data gaps.

[15] In order to understand the possible mechanisms responsible for the different scintillation levels recorded, theoretical PSDs were calculated according to the theory developed by *Uscinski* [1968] and *Booker and MajidiAhi* [1981]. Both experimental and theoretical PSDs were presented in terms of fractional PSDs (in units of S_4^2/Hz), which essentially are the usual PSD normalized by the square of the average received intensity. The integration of the fractional PSD immediately gives S_4 [*Booker and MajidiAhi*, 1981; *Vats et al.*, 1981; *Forte*, 2008]. A key parameter in this calculation is the mean square fractional fluctuation of the ionization spatial density. This parameter was calculated by estimating the mean square electron content fluctuation along a particular raypath [*Vats et al.*, 1981; *Forte*, 2008]. This method, however, posed a limitation in the analysis because in the presence of strong C/N_0 fluctuations, the TEC variations measured on the ground include an unwanted enhancement due to phase scintillation effects. This may lead to overestimates of the phase variance in strong scatter. A better estimate of the phase variance could likely be obtained following the method devised in *Carrano et al.* [2011]. The estimate was indeed obtained by using L1 phase alone (since L2 is affected more strongly by diffraction) after removing the geometric Doppler and using precise ephemeris together with careful detrending of the residual [*Carrano et al.*, 2011].

[16] Assuming the estimate of the mean square electron content fluctuation based on TEC variations (bearing in mind the limitations of such an approach), the results of this calculation are shown in Figure 10 and correspond to the conditions characterizing the raypath of PRN30 (see Figures 1–2). Figure 10a corresponds to the theoretical fractional PSD with a spectral index of $p = 3$, while Figure 10b corresponds to a spectral index of $p = 5$. Data gaps at high fluctuation frequencies were due to limitation in the numerical integration method utilized. The color scale in Figure 10 is such that blue corresponds to 10^{-8} while red to 10^{3} with

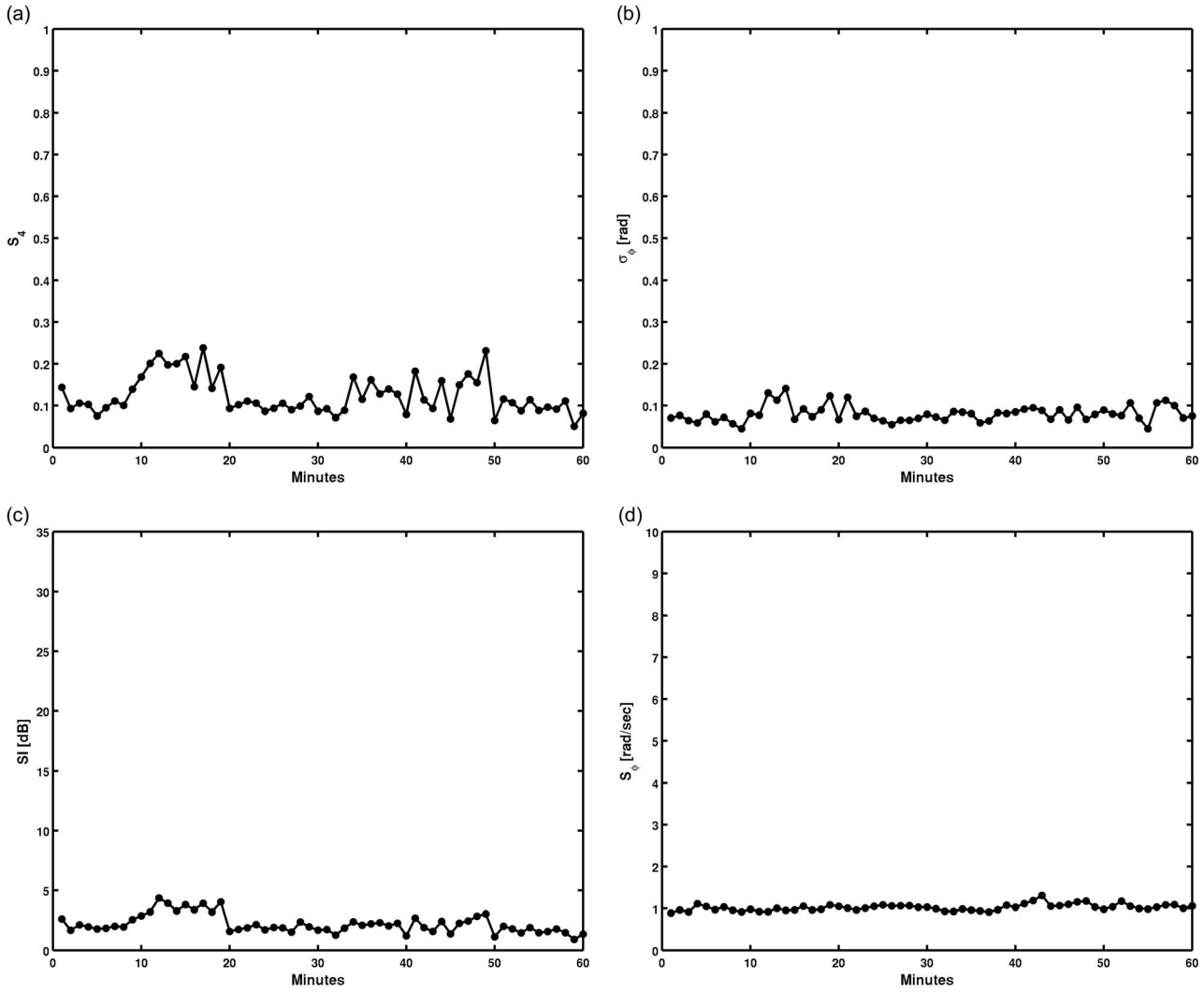

Figure 6. The scintillation indices S_4, σ_ϕ, SI, and S_ϕ for PRN22 at L1 between 20:00LT and 21:00LT as observed from Bandung on 6 April 2005.

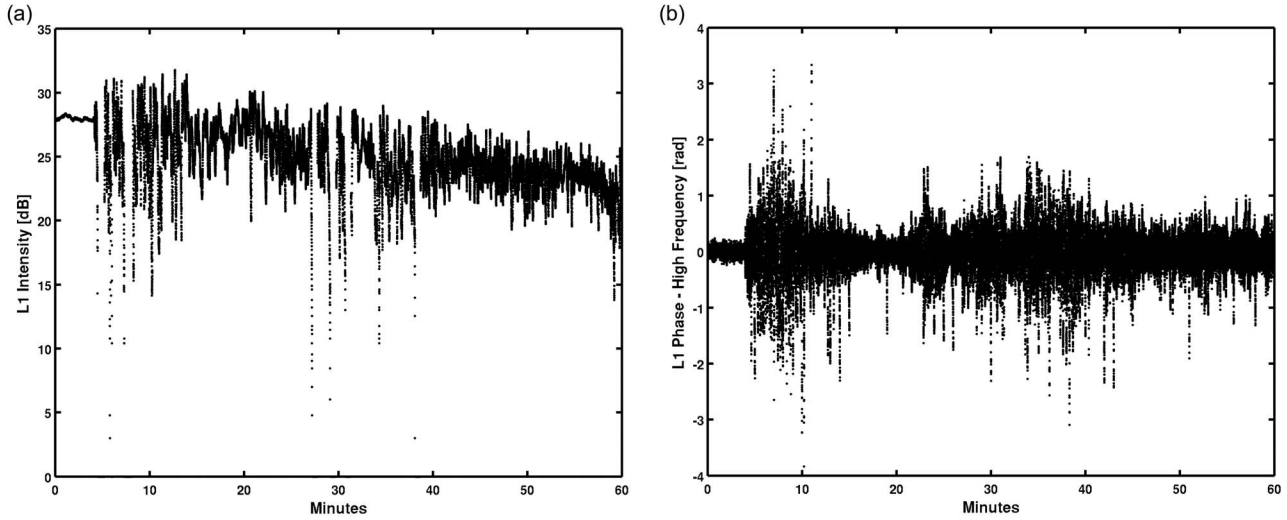

Figure 7. The non-detrended intensity and the detrended phase for PRN30 at L1 between 18:00LT and 19:00LT as observed from Bandung on 6 April 2005.

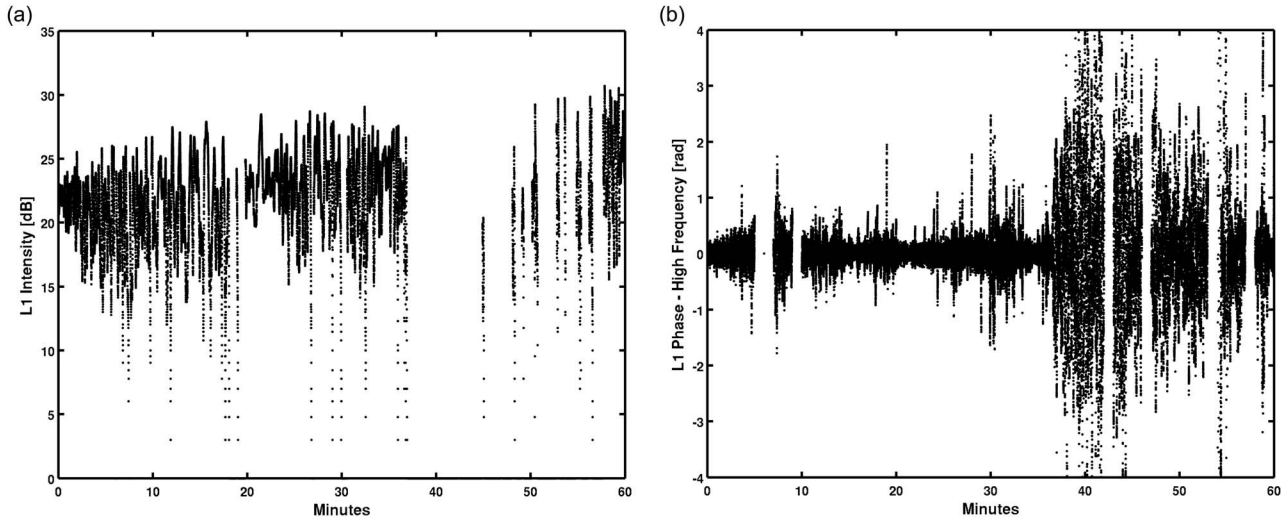

Figure 8. The non-detrended intensity and the detrended phase for PRN01 at L1 between 20:00LT and 21:00LT as observed from Bandung on 6 April 2005.

units of S_4^2/Hz. What matters in the comparison between Figures 9 and 10 are not absolute values of the PSDs but their relative changes within each of the figures for the identification of possible spectral broadening. The particular values of $p = 3$ and $p = 5$ for the spectral index proved the most representative cases. The case corresponding to $p = 2$ did not show significant spectral broadening, while the numerical integration for the theoretical PSD corresponding to $p = 4$ did not converge over all frequencies, preventing from its reconstruction over a significant interval of wave numbers. In the cases of $p = 3$ and $p = 5$, spectral broadening was evident in the presence of high scintillation activity, i.e., around minutes 5 and 30 (see Figures 1 and 2). The spectral broadening was observed on both theoretical spectra (Figure 10) and experimental spectra (Figure 9a). Nevertheless, the theoretical spectra corresponding to a spectral index of $p = 3$ showed a slightly larger contribution at higher wave numbers (Figure 10a) than what appeared in the case of the spectral index of $p = 5$ (Figure 10b).

[17] A further comparison was provided in Figure 11, where theoretical and experimental spectra were compared for the same scintillation level (characterized by low and high S_4 values). Figure 11a shows the experimental spectra, while Figure 11b shows the theoretical spectra corresponding to a spectral index $p = 3$ and Figure 11c shows the case for $p = 5$ under same conditions as in Figure 11a. In all plots, the solid lines correspond to low scintillation conditions at minute 18:02LT when $S_4 = 0.1$ for PRN30, while the dashed lines correspond to high scintillation activity at minute 18:05LT when $S_4 = 1.1$ for signals from the same satellite. The theoretical spectra were also plotted against the temporal frequencies on the basis of the satellite motion only as the ionospheric plasma drift was unknown. The difference in the numerical values between observed and calculated spectra was due to (1) discrepancies between experimental parameter settings (e.g., receiver gains) and constant values involved in the theoretical calculations, (2) the use of a simple power law model for the phase fluctuations, (3) the use of an estimate for the phase variance as determined from the TEC fluctuations. In the case of a spectral index of $p = 3$ a lowering and a spreading of the calculated PSD toward both high and low spatial frequencies in the high scintillation case was observed (Figure 11b). At high spatial frequencies the roll-off of the intensity spectrum was approximately gaussian and this is a typical situation when refractive scattering dominates over diffractive scattering. The gaussian roll-off shows the existence of a fine structure created in the reception plane by refractive scattering [*Booker and MajidiAhi*, 1981; *Uscinski*, 1968]. In the case of a spectral index $p = 5$ (Figure 11c) an expansion toward higher wave numbers together with an increase of the PSD was observed, which appeared more closely related to what observed experimentally (Figure 11a). Figure 12 shows the comparison between experimental values for S_4 measured over PRN30 (full dots) and the theoretical values for S_4 obtained by integrating the PSDs shown in Figure 10 for $p = 3$ (crosses) and $p = 5$ (open circles). The theoretical values for $p = 3$ appeared almost constant, while those for $p = 5$ showed a trend similar to the experimental values, although S_4 was underestimated during strong and saturating scintillation levels.

[18] In the classical weak scattering theory the scintillation indices depend, amongst others, on a geometrical factor G which is capable of producing enhancements in the indices due to a raypath geometry accounting for propagation along the largest aspect ratio dimension [*Rino and Matthews*, 1980; *Rino and Owen*, 1980]. However, previous analyses showed that such a parameter is not enough in the case of GPS raypaths to explain similar enhancements in the scintillation indices [*Forte and Radicella*, 2004; *Forte*, 2007] at high latitudes, because the orbits of GPS satellites cannot produce raypath aligned within L shells. This is even more the case at low latitudes for obvious geometrical considerations. The enhancements in scintillation activity observed along the raypath from PRN30 cannot be explained by means of the classical weak scattering theory solely on the basis of the geometrical factor G at least.

[19] Similar results were obtained in the past by refining the weak scattering theory through the use of numerical

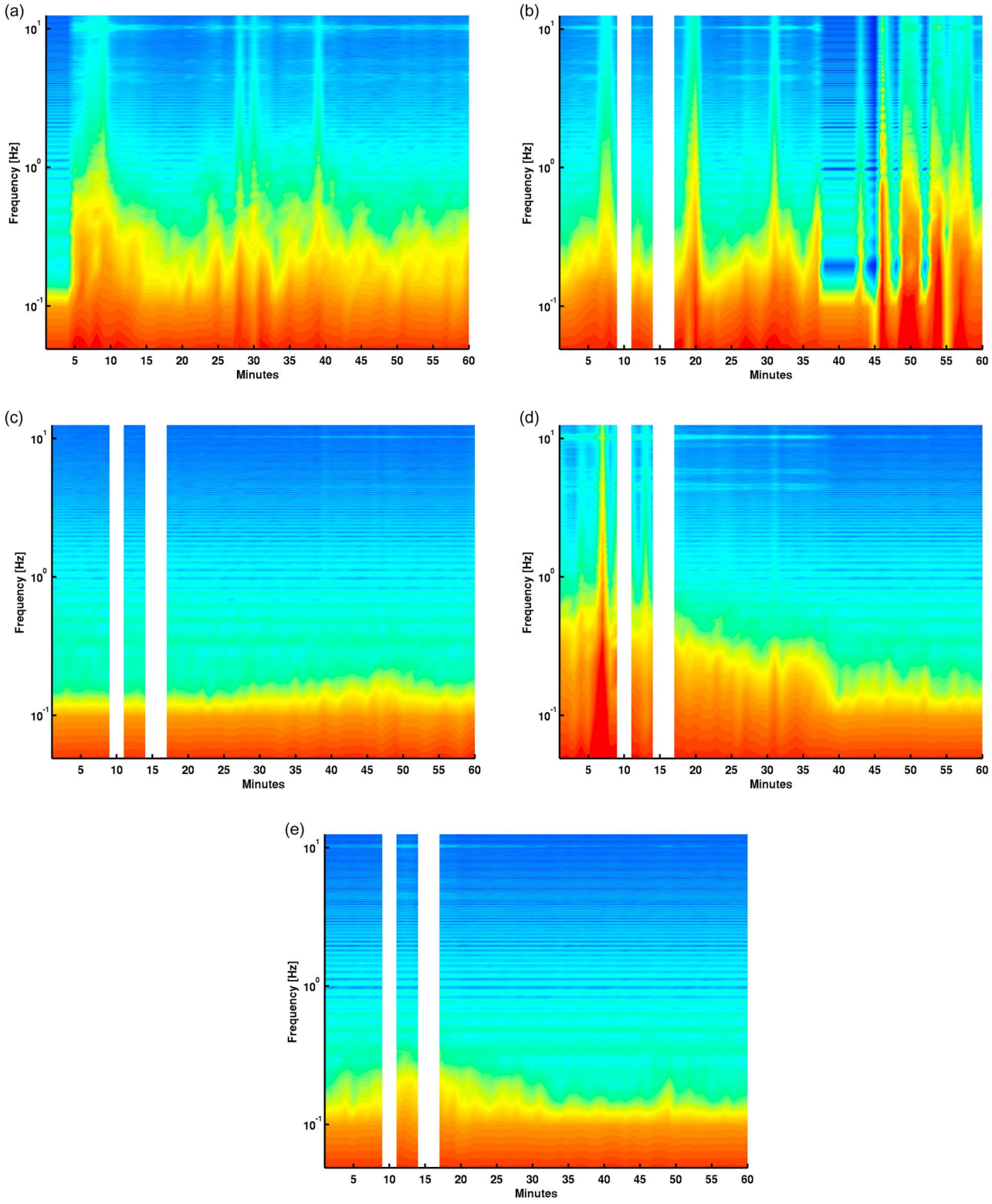

Figure 9. Temporal behavior of experimental PSD. (a) PRN30, (b) PRN01, (c) PRN03, (d) PRN14, and (e) PRN22.

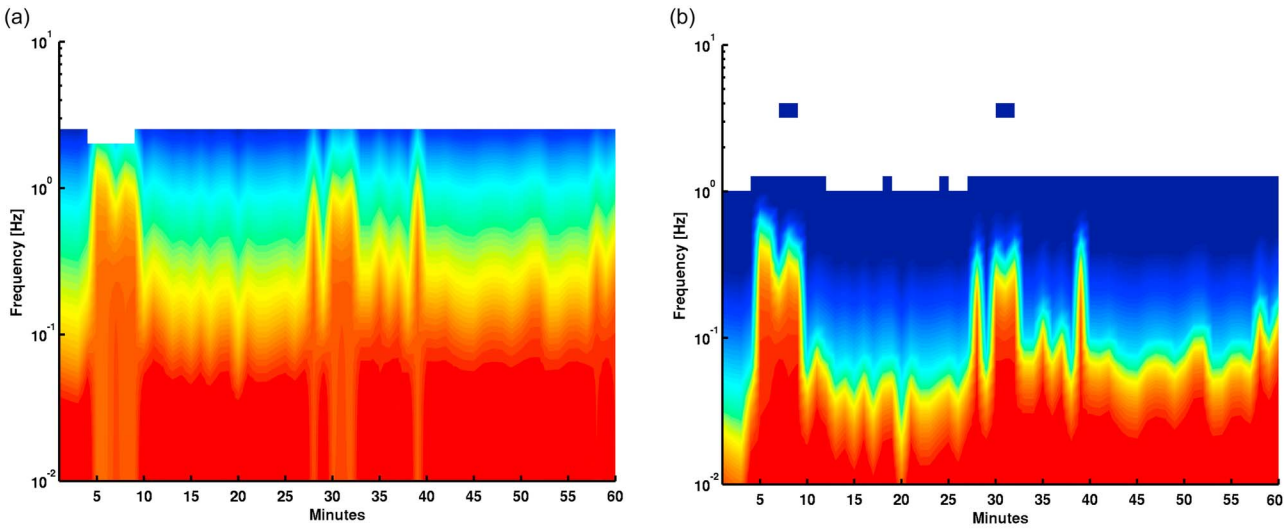

Figure 10. Temporal behavior of theoretical PSD corresponding to conditions on PRN30 (Figure 3a); (a) $p = 3$ and (b) $p = 5$.

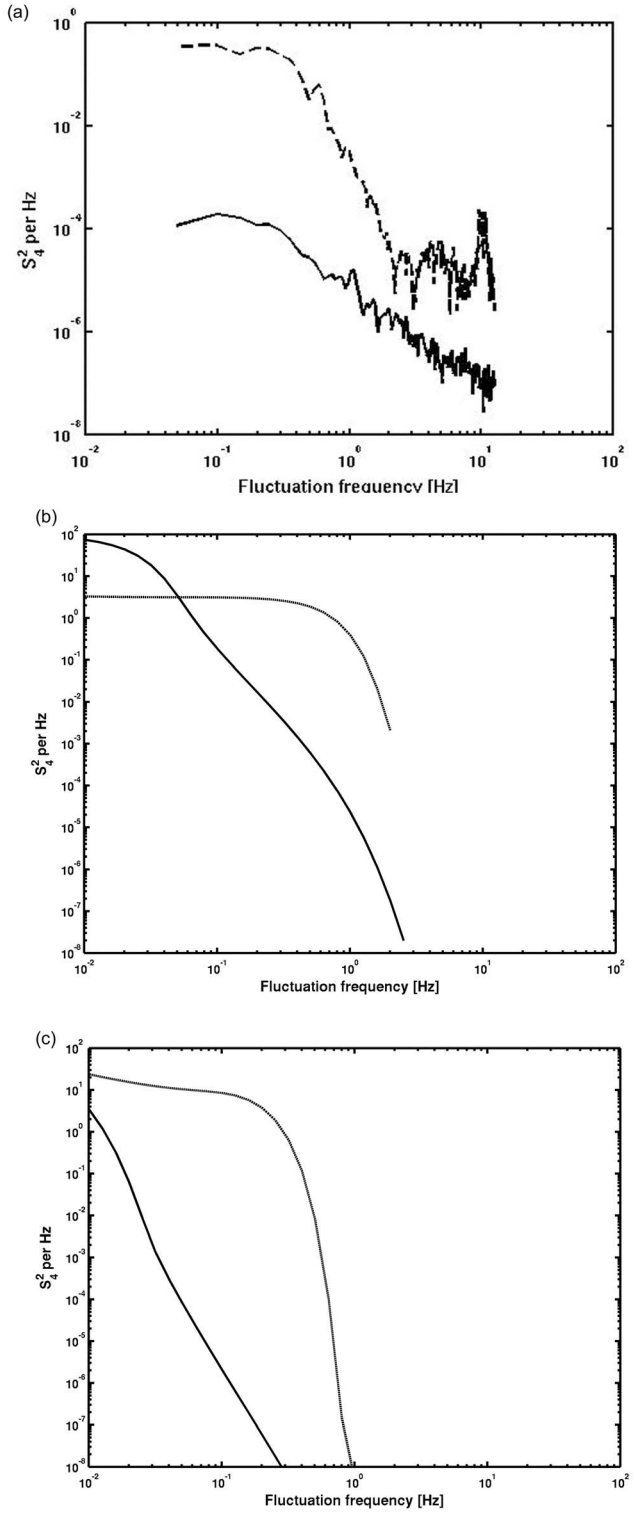

Figure 11. (a) Experimental PSD for minutes 18:02LT (S_4 = 0.1, solid line) and 18:05LT (S_4 = 1.1, dashed line) as observed from Bandung on 6 April 2005. Theoretical PSD corresponding to minutes 18:02LT and 18:05LT for spectral indices (b) p = 3 and (c) p = 5.

methods for calculating a series expansion of the intensity spectral density function (SDF) based on a 1-D phase SDF [*Rino and Owen*, 1984]. These simulations were applied not only to a single component power law, but also extended to a two-component power law for the phase SDF [*Franke and Liu*, 1983; *Rino and Owen*, 1984; *Franke and Liu*, 1985]. The assumption of a two-component power law phase SDF was based on in-situ measurements made at equatorial latitudes [*Basu et al.*, 1983].

[20] The improved weak scattering description based on a two-component power law seemed to include features such as the spectral broadening similar to what was observed in the case study presented here [*Franke and Liu*, 1983, 1985]. Here, only the refractive scattering theory developed by *Uscinski* [1968] and *Booker and MajidiAhi* [1981] was used to provide a possible explanation of the events observed. The use of weak scattering with two-component power law was investigated for example in *Forte* [2007] but it was not attempted here.

[21] The spectral modifications and broadening observed on the experimental data seemed to indicate scattering mechanisms probably different from a weak scattering type. The present analysis certainly contained limitations such as the assumption of a single phase screen, a single strong scattering rather than multiple scattering [*Booker et al.*, 1985; *Bhattacharyya and Yeh*, 1988], a single rather than two (or multiple) components power law [*Franke and Liu*, 1983; *Basu et al.*, 1983], limitations in the numerical integration methods. The observations presented here were supposed to report cases of strong scintillation observed at L band by means of GPS signals at low latitudes, which might be due to possible alternative scattering mechanisms in addition to weak scattering (e.g., refractive scattering).

[22] In the particular case study presented here and, overall, in all case studies dealing with GPS measurements, the estimate of the power spectral densities can potentially be inaccurate under very strong conditions. The energy is

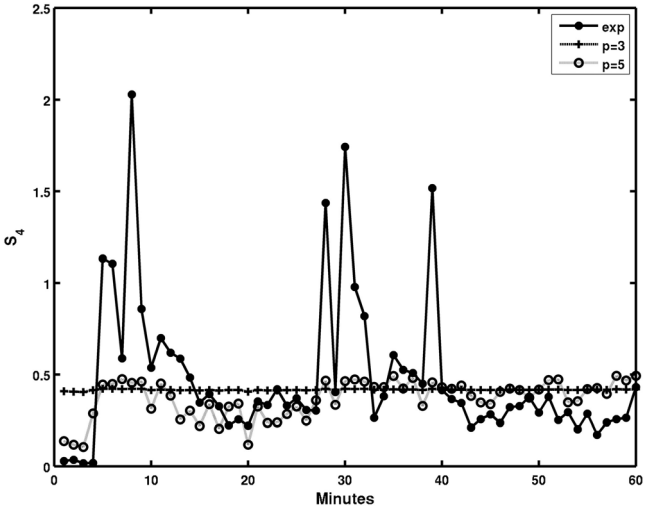

Figure 12. Comparison between experimental and theoretical S_4 values corresponding to the case of PRN30 observed between 18:00LT and 19:00LT. Full dots represent experimental values, crosses refer to a spectral index p = 3, while the open circles refer to a spectral index p = 5.

distributed over a range of frequencies centered around the nominal carrier (for instance L1). During the scattering onto electron density inhomogeneities, the energy is scattered according to its frequency distribution. Moreover, the signal intensity and phase are not measured directly within GPS receivers (including GPS ionospheric monitors) but reconstructed through phase locked loops (PLL). Along this chain of processes the accuracy in the estimate of the spatial SDF can be deteriorated. For instance, the PLL might work nonlinearly in the presence of moderate to high scintillation events. All the above limitations need to be taken into account.

4. Conclusions

[23] A short sample of GPS based experimental data collected at low latitudes were analyzed. Different levels of scintillation activity were observed including low, moderate, high, and saturating scintillation ($S_4 \sim 1$). Spectral modifications and broadening were observed in the presence of high scintillation activity, particularly in correspondence of saturating scintillation levels.

[24] A possible interpretation of the spectral modifications observed in the experimental data was attempted on the basis of a refractive scattering approach, where the waves are scattered by plasma density spatial inhomogeneities larger than the Fresnel scale. The formulation of the refractive scattering approach developed in *Uscinski* [1968] and *Booker and MajidiAhi* [1981] contained the diffractive scattering approach. However, a strong assumption was made in that approach: i.e., the multiple scattering was approximated by a single strong scattering [*Booker et al.*, 1985; *Bhattacharyya and Yeh*, 1988].

[25] Despite the limitations in the theoretical calculations, the spectral modifications and broadening observed on the experimental data seemed to indicate scattering mechanisms probably different from a weak type of scattering. The use of multiple scattering together with multiple components power law might possibly suggest further improvements to the modeling of radio wave propagation through an extended medium.

[26] **Acknowledgments.** This research was supported by a Marie Curie Intra European Fellowship within the 7th European Community Framework Programme. The author wishes to thank N. Jakowski from the Deutsches Zentrum für Luft- und Raumfahrt (German Aerospace Center, Institute of Communications and Navigation, Neustrelitz) for kindly sharing some intervals of experimental data collected at Bandung. The author is deeply thankful to the reviewers who provided significant contributions to the improvement of this paper.

References

Basu, S., Su. Basu, J. P. McClure, W. B. Hanson, and H. E. Whitney (1983), High resolution topside in situ data of electron densities and VHF/GHz scintillations in the equatorial region, *J. Geophys. Res.*, *88*(A1), 403–415.

Bhattacharyya, A., and K. C. Yeh (1988), Intensity correlation function for waves of different frequencies propagating through a random medium, *Radio Sci.*, *23*(5), 791–808.

Booker, H. G., and G. MajidiAhi (1981), Theory of refractive scattering in scintillation phenomena, *J. Atmos. Terr. Phys.*, *43*(11), 1199–1214.

Booker, H. G., J. A. Ferguson, and H. O. Vats (1985), Comparison between the extended medium and the phase-screen scintillation theories, *J. Atmos. Terr. Phys.*, *47*, 381–399.

Briggs, B. H., and I. A. Parkin (1963), On the variation of radio star and satellite scintillations with zenith angle, *J. Atmos. Terr. Phys.*, *25*, 339–365.

Carrano, C. S., K. M. Groves, and R. G. Caton (2011), Accuracy of phase screen models using deterministic screens derived from GPS and ALTAIR measurements, paper presented at Ionospheric Effects Symposium, U.S. Off. of Nav. Res., Alexandria, Va., 17–19 May.

Crain, C. M., H. G. Booker, and J. A. Ferguson (1979), Use of refractive scattering to explain SHF scintillations, *Radio Sci.*, *14*(1), 125–134.

Forte, B. (2005), Optimum detrending of raw GPS data for scintillation measurements at auroral latitudes, *J. Atmos. Sol. Terr. Phys.*, *67*, 1100–1109.

Forte B. (2007), On the relationship between the geometrical control of scintillation indices and the data detrending problems observed at high latitudes, *Ann. Geophys.*, *50*(6), 699–706.

Forte, B. (2008), Refractive scattering evidence from multifrequency scintillation spectra observed at auroral latitudes, *Radio Sci.*, *43*, RS2012, doi:10.1029/2007RS003715.

Forte, B., and S. M. Radicella (2004), Geometrical control of scintillation indices: What happens for GPS satellites, *Radio Sci.*, *39*, RS5014, doi:10.1029/2002RS002852.

Franke, S. J., and C. H. Liu (1983), Observations and modeling of multifrequency VHF and GHz scintillations in the equatorial region, *J. Geophys. Res.*, *88*(A9), 7075–7085.

Franke, S. J., and C. H. Liu (1985), Observations and modelling of multifrequency scintillation, *Radio Sci.*, *20*(3), 403–415.

Fremouw, E. J., R. L. Leadabrand, R. C. Livingston, M. D. Cousins, C. L. Rino, B. C. Fair, and R. A. Long (1978), Early results from the DNA Wideband Satellite Experiment–Complex signal analysis, *Radio Sci.*, *13*(1), 167–187.

Humphreys, T. E., M. L. Psiaki, J. C. Hinks, B. O'Hanlon, and P. M. Kintner (2009), Simulating ionosphere-induced scintillation for testing GPS receiver phase tracking loops, *J. IEEE Sel. Top. Signal Process.*, *3*(4), 707–715, doi:10.1109/JSTSP.2009.2024130.

Rino, C. L. (1979a), A power law phase screen model for ionospheric scintillation 1. Weak scatter, *Radio Sci.*, *14*(6), 1135–1145.

Rino, C. L. (1979b), A power law phase screen model for ionospheric scintillation 2. Strong scatter, *Radio Sci.*, *14*(6), 1147–1155.

Rino, C. L., and S. J. Matthews (1980), On the morphology of auroral zone radio wave scintillation, *J. Geophys. Res.*, *85*, 4139–4151.

Rino, C. L., and J. Owen (1980), The structure of localized nighttime auroral zone scintillation enhancements, *J. Geophys. Res.*, *85*(A6), 1941–1948.

Rino, C. L., and J. Owen (1984), Numerical simulations of intensity scintillation using the power law phase screen model, *Radio Sci.*, *19*(3), 891–908.

Uscinski, B. J. (1968), The multiple scattering of waves in irregular media, *Phil. Trans.*, *A262*, 609–640.

Van de Kamp, M. M. J. L., and P. S. Cannon (2009), Spectra of equatorial total electron content derived from GPS signals, *Ann. Geophys.*, *27*, 2205–2214.

Van Dierendonck, A. J., Q. Hua, and J. Klobuchar (1993), Ionospheric scintillation monitoring using commercial single frequency C/A code receivers, paper presented at Sixth International Technical Meeting of the Satellite Division of the Institute of Navigation GPS 93, Salt Lake City, Utah, 22–24 Sept.

Vats, H. O., H. G. Booker, and G. MajidiAhi (1981), Quantitative explanation of strong multi-frequency intensity scintillation spectra using refractive scattering, *J. Atmos. Terr. Phys.*, *43*(12), 1235–1241.

Whitney, H. E., and M. Chester (1968), A proposed index for measuring ionospheric scintillation, *U. S. Air Force Cambridge Res. Lab. Environ. Res. Pap.*, *284*, 68-0138.

Yeh, K. C., and C. H. Liu (1982), Radio wave scintillations in the ionosphere, *Proc. IEEE*, *70*(4), 324–360.